Elastic scattering of 200 keV electrons in elemental solids: experimental observation of atomic-number-dependent oscillatory behavior

2009 J. Phys.: Condens. Matter 21 155402

(http://iopscience.iop.org/0953-8984/21/15/155402)

J. Phys.: Condens. Matter **21** (2009) 155402 (5pp) doi:10.1088/0953-8984/21/15/155402

Elastic scattering of 200 keV electrons in elemental solids: experimental observation of atomic-number-dependent oscillatory behavior

Konstantin Iakoubovskii and Kazutaka Mitsuishi

Quantum Dot Research Center, National Institute for Materials Science, 3-13 Sakura, Tsukuba 305-0005, Japan

Received 8 December 2008, in final form 25 February 2009
Published 20 March 2009
Online at stacks.iop.org/JPhysCM/21/155402

Abstract

Mean free path of elastic electron scattering λ_{el} has been measured with a 200 keV transmission electron microscope for a wide range of stable elemental solids. An oscillating behavior versus atomic number Z has been revealed, such that, within one row of the periodic table, λ_{el} exhibits minimum (maximum) for elements with completed (empty) outer d shells. These $\lambda_{el}(Z)$ oscillations are attributed to Z dependence of the atomic density, and their importance for the interpretation of electron microscope images is demonstrated.

(Some figures in this article are in colour only in the electronic version)

1. Introduction

Since the pioneering work by Rutherford [1], elastic scattering of electrons by atoms has been a subject of numerous studies and reviews (see, e.g., books by Egerton [2] and Spence [3]). The scattering is traditionally evaluated by its cross section σ; it depends on several experimental parameters, and this paper will focus on the variation of σ with the atomic number Z.

The Rutherford theory predicted the relation $\sigma(Z) \sim Z^2$. However, it neglected the electronic structure of the scattering atom, and thus the Z^2 law is only a first approximation. Over decades, calculations have gradually included numerous corrections and finalized in a complex $\sigma(Z)$ dependence (blue solid squares in figure 4 introduced later in the text), which can be fitted quite well by a $\sigma(Z) \sim Z^{1.5}$ function. Those σ values have been calculated using a Dirac partial wave method with screened potentials obtained from Dirac–Hartree–Fock atomic electron densities [4]. The exchange and nuclear size effects have been accounted for.

Practical applications of electron scattering, and in particular of its $\sigma(Z)$ dependence, are numerous. One of the most important is transmission electron microscopy (TEM), and especially high angle annular dark field (HAADF or 'Z-contrast') imaging [5, 6]. The latter technique, inherent to scanning TEM (STEM), provides artifact-free, high-contrast pictures; it has single-atom sensitivity [7, 8] and is therefore one of the most valued TEM methods. Analysis of the HAADF images crucially relies on the atomic number dependence of the electron scattering.

Note, however, that TEM objects are not atoms but solids. Arranging atoms into a crystalline solid brings two extra contributions: diffraction and scattering by the atomic vibrations called thermal diffuse scattering (TDS). As a result, the total scattering is a complex function of the microscope parameters and of the atomic structure, orientation and thickness t of a particular TEM sample. Systematic control over all those parameters in the experiment is extremely difficult, and thus only a few studies have been reported thus far [9, 10]. Meanwhile, calculations predicted [11] that the scattering intensity should behave as Z^a, where a varies between 1.6 and 1.9 depending on the electron optics geometry.

If diffraction effects are weak then the normalized scattering intensity I/I_0 can be evaluated [2] with a usual relation $I/I_0 = 1 - \exp(-t/\lambda)$ and the mean free path of the scattering λ related to σ as $1/\lambda = N\sigma$. Here $N = \rho/(Am)$ is the atomic density, ρ is mass density, A is the dimensionless atomic mass and m is the proton mass. Using those expressions, Bals *et al* [9] have experimentally obtained $\sigma(Z) \sim Z^{1.47}$ dependence and their σ values were consistent with the atomic calculations [4]. However, measurements were performed on three solids only (Si, GaN and Au), at different microscope settings, and thus are hardly representative.

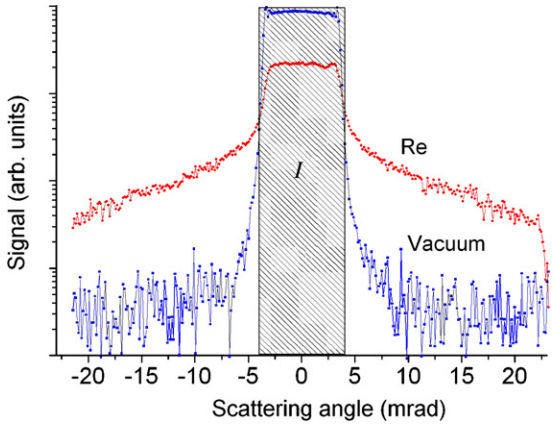

Figure 1. An example of angular-resolved electron scattering measurement (note the logarithmic scale). The reference spectrum (vacuum) is dominated by unscattered electrons in the range −4 to 4 mrad. Insertion of a sample (rhenium foil) induces scattering, which is measured as the integrated intensity ratio $1 - I_{\mathrm{Re}}/I_{\mathrm{Vacuum}}$.

In this paper, we report systematic measurements of λ_{el} in a wide range of solids. Instead of a monotonic variation an oscillatory $\lambda_{\mathrm{el}}(Z)$ behavior is revealed and explained by Z dependence of the atomic density.

2. Experimental details

2.1. Measurements

Measurements were performed with a JEOL 200 keV high-vacuum 2500SES STEM equipped with an Enfina electron energy loss (EEL) spectrometer and a hexapole spherical aberration corrector [12–14]. The microscope parameters, such as convergence semiangle (4 mrad), camera length and other settings, were fixed and only the samples have been exchanged. The EEL camera is set up in the diffraction plane which allows angular-resolved measurements of electron scattering as follows (see figure 1).

First, a circular beam is aligned to the camera center. The EEL spectrometer is turned to the 'zero-dispersion mode' and the central cross section of the image is recorded as an angular-resolved spectrum. In the zero-dispersion mode the dispersing magnet is switched off and the EELS camera operates as a diffraction imaging device [2, 5]. Angular calibration is performed using diffraction from crystalline Si. Insertion of a sample results in wide-angle scattering, which is measured via the ratio of the integrated intensities in the −4 to 4 mrad range as $1 - I_{\mathrm{Sample}}/I_{\mathrm{Vacuum}}$. This scattering is hereafter called 'elastic', and further, in section 3.1, its individual contributions are discussed. Note that inelastic scattering has a rather narrow ($\ll$1 mrad) angular distribution [2, 16] and it is therefore mostly included in the unscattered beam.

Then the energy dispersion is switched on and an EEL spectrum is recorded from the same sample area yielding the relative thickness t/λ_{in} [2, 15, 16]. The latter is converted into the absolute thickness using the tabulated values of the inelastic mean free path λ_{in} [15, 16]. Finally, the mean free path of elastic scattering is deduced as $\lambda_{\mathrm{el}} = -t/\ln(I_{\mathrm{Sample}}/I_{\mathrm{Vacuum}})$.

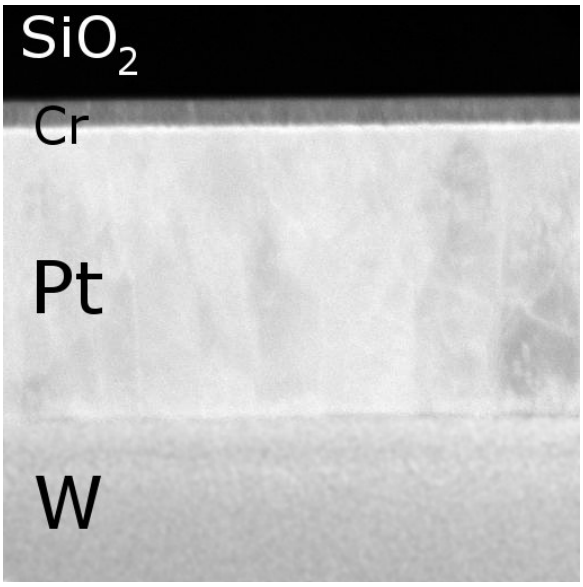

Figure 2. HAADF image of a layered structure where polycrystalline Pt and Cr layers are sandwiched by amorphous tungsten and SiO_2. Image width is 300 nm.

2.2. Sample preparation

Thin sample areas ($t/\lambda_{\mathrm{in}} < 1$) were selected in order to reduce multiple, especially multiple inelastic, scattering, which could have wide angular distribution and thus mix up into elastic scattering. In order to minimize diffraction effects, single-crystalline samples were avoided and disordered samples studied wherever possible. The latter were prepared using various techniques including sputtering or thermal evaporation onto a cooled substrate, high velocity impact and ion implantation. For example, amorphous xenon particles were produced by Xe^+ implantation of Al foils [17].

When amorphous samples were not available, nanocrystalline materials were studied instead. Because of diffraction, the scattering intensity was varying from grain to grain, but ample spatial averaging brought consistent results (see figure 2).

The Ag/I sample was prepared by electron irradiation of AgI powder for several hours inside the microscope. In this process we used the well-known property of AgI—a traditional photographic material—to develop Ag-rich and I-rich grains under exposure to light or electrons, and a long irradiation was required to stabilize the sample.

The GaAs nanocones were grown by droplet epitaxy [18]: Ga droplets were deposited on a GaAs substrate. They were then reacted with As_4 gas, thus resulting in GaAs growth over Ga. A cross-sectional TEM sample was prepared by focused ion beam cutting. The cones were covered with an amorphous carbon layer in order to protect them from the 30 keV Ga beam.

3. Results and their analysis

3.1. Material dependence of elastic scattering

Figure 3 summarizes the measured values of λ_{el} (solid squares). Corresponding $\lambda_{\mathrm{in}}(Z)$ dependence [15] is also shown

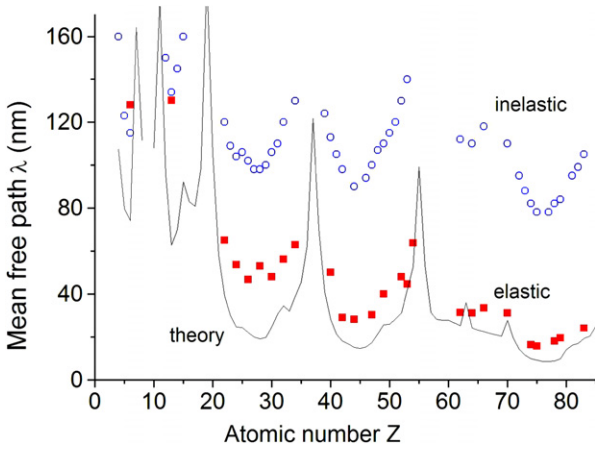

Figure 3. Solid squares present the mean free path of elastic scattering λ_{el} of 200 keV electrons. Open circles correspond to inelastic values λ_{in} [15]. The solid line represents $1/N\sigma$ function, containing the calculated atomic cross sections σ [4] and the atomic density N (see figure 4).

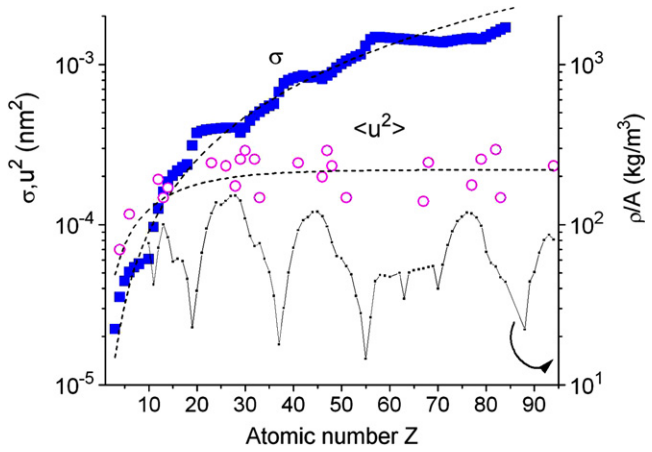

Figure 4. Solid squares present calculated [4] cross sections σ corresponding to elastic scattering of 200 keV electrons by single atoms; this $\sigma(Z)$ dependence is approximated by a $Z^{1.5}$ increase (dashed curve). Open circles show experimental [22, 23, 19–21, 24–30] mean-square atomic displacements in elemental solids $\langle u^2\rangle$ fitted with a $1-\exp(-Z/12)$ function. The bottom curve is the density ρ divided by the atomic mass A.

for reference. Comparison of λ_{el} and λ_{in} values suggests that the elastic component should dominate scattering of high-energy electrons for most inorganic solids. Figure 3 reveals that, in a similar fashion, λ_{el} and λ_{in} are not monotonic but oscillatory functions of Z for $Z > 20$. The behavior of $\lambda_{in}(Z)$ has been explained previously [15], and in the following paragraphs we shall attempt an understanding the oscillatory $\lambda_{el}(Z)$ dependence for $Z > 20$.

Let us discuss the physical processes associated with the λ_{el} values of figure 3. Two major contributions will be considered: elastic scattering and TDS. We shall neglect multiple scattering, such as elastic–inelastic, etc, that is partly justified by the small thickness of our samples ($t \leqslant \lambda_{el} < \lambda_{in}$). We shall also ignore diffraction effects relying on the disordered structure of most of our samples. Consequently, elastic scattering can be treated as independent atomic scattering events and the expression $1/\lambda = N\sigma$ can be used, where σs are the calculated [4] atomic cross sections plotted in figure 4.

As to TDS, the corresponding scattering potential is strongly localized [10] at the vibrating atom. Therefore again, collective effects can be ignored and the scattering associated with independent movements of individual atoms.

In essence, TDS can be viewed as elastic scattering modified by the atomic vibrations. Therefore, it is instructive to compare, in figure 4, the published values and their Z dependences of the calculated [4] elastic cross section σ and of the experimental mean-square atomic displacement $\langle u^2\rangle$.

The $\langle u^2\rangle$ values can be deduced from various measured quantities, such as thermal expansion, thermal conductivity, extended x-ray absorption fine structure (EXAFS) and the widths of the x-ray or neutron diffraction peaks. The associated measurements have different characteristic frequencies, thus yielding unequal $\langle u^2\rangle$ values [22, 23]. Additional confusion arises from usage of various formulae relating the Debye–Waller factor B and $\langle u^2\rangle$: $B = 8\pi^2\langle u^2\rangle$ or $B = 8\pi^2\langle u^2\rangle/3$. Nevertheless, we could summarize in figure 4 some of the appropriate $\langle u^2\rangle$ values [22, 23, 19–21, 24–30], most of which were obtained by x-ray and a few by neutron diffraction.

Comparison of the σ and $\langle u^2\rangle$ values suggests that TDS can be ignored in explaining the $\lambda(Z)$ dependence, especially for large Z. Thus we may compare the experimental λ_{el} data of figure 3 with the $1/N\sigma$ values of figure 4, as shown by the solid line in figure 3. A good agreement with experiment is observed. The measured values are somewhat larger which can be partly explained by the fact that part (<4 mrad) of the scattering has been discarded in our measurements (see the acknowledgment for another reason). Note that the atomic density N varies much stronger with Z than σ or $\langle u^2\rangle$ (see figure 4), and thus the oscillatory $\lambda_{el}(Z)$ behavior can be attributed to the atomic density.

3.2. *Importance of* $\lambda_{el}(Z)$ *dependence for electron microscopy*

The results of figure 3 are important for electron microscopy, and especially for the increasingly popular HAADF imaging [5, 6]. Given the constant thickness, brighter regions in HAADF pictures are commonly associated with heavier elements [7–9, 31–34]. However, data of figures 3 and 4 suggest that it is not the atomic number but atomic density that determines the contrast, and the density oscillates with the atomic number.

Supportive examples are shown in figures 5 and 6. In both examples, the HAADF detector semiangle was set at >100 mrad. In TEM images, it is important to distinguish scattering contrast from thickness contrast. Therefore, figure 5 contains a thickness map obtained by Kramers–Kronig analysis of EEL measurements [2, 15, 16]. It demonstrates that thickness variation had a minor effect on the grain contrast. As to figure 6, because of the carbon coating required for sample preparation, it was not possible to obtain a reliable EEL thickness map. However, scanning electron microscopy observations revealed a smooth conical shape of that GaAs

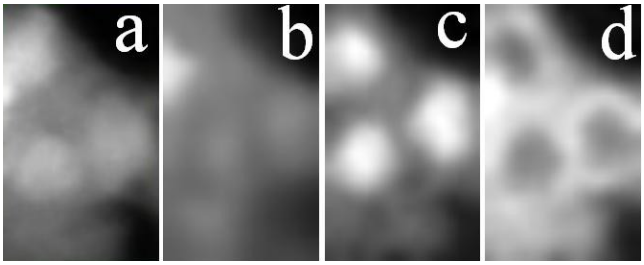

Figure 5. Panel (a) shows HAADF image (image width 30 nm) of Ag/I structure obtained by electron irradiation of AgI powder. Panel (b) is a thickness map measured by EEL spectroscopy where black to white contrast corresponds to the range 0–20 nm. Panels (c) and (d) show maps of silver and iodine concentrations (in arbitrary units), respectively, obtained using the M_{45} EEL edges. Note that silver grains appear brighter than iodine grains in the HAADF image (a).

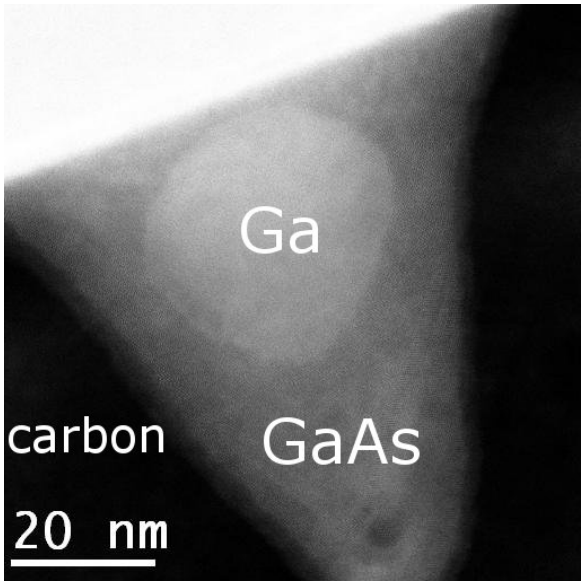

Figure 6. HAADF image of a GaAs cone grown by droplet epitaxy [18]. The cone still contains liquid Ga precursor, which appears brighter than surrounding GaAs.

structure, and thus the sharp contrast of the embedded droplet in figure 6 cannot be attributed to the thickness variation.

Figures 5 and 6 reveal that materials composed of lighter atoms, but having larger atomic density, appear brighter in HAADF images. In particular, in figure 5(a), silver ($Z = 47$, $\rho = 10.5$ g cm^{-3}) is brighter than iodine ($Z = 53$, $\rho \simeq 5$ g cm^{-3}), and in figure 6, Ga ($Z = 31$, $\rho = 5.9$ g cm^{-3}) is brighter than GaAs (average $Z = 32$, $\rho = 5.3$ g cm^{-3}).

4. Summary and conclusions

This paper reports systematic measurements of mean free path of elastic scattering λ_{el} of 200 keV electrons by a wide range of (mostly disordered) elemental solids. Comparison with previously reported [15] inelastic values λ_{in} reveals that $\lambda_{el} < \lambda_{in}$ for most inorganic solids, and thus the elastic component would likely dominate scattering of high-energy electrons. Oscillations of λ_{el} with atomic number Z are discovered and associated with Z dependence of the atomic density. This non-monotonic behavior should be considered when analyzing TEM images. Currently, their interpretation relies on the smooth Z^a variation of the scattering, which might be true for individual atoms in a solid, but not for different materials. In the latter, atomic density of the sample constituents should be taken into account.

Acknowledgments

One of the referees has pointed out that, whereas we used elastic cross sections calculated for free atoms, the core electron density in a solid is more contracted, which reduces the total elastic cross section σ. Using a simple muffin-tin model, the referee calculated a 10% reduction of σ for tin ($Z = 50$). Hence, if elastic cross sections were calculated using atomic electron densities more appropriate to the solid state, the theoretical line in figure 4 would rise, providing slightly better agreement with the experiment.

This research was partly supported by the Ministry of Education, Science, Sports, and Culture (MEXT) through the Grant-in-Aid for Young Scientists (B) 2005 17710120-6816, the World Premier International Research Center Initiative on Materials Nanoarchitronics and the Nuclear Research Project.

References

[1] Rutherford E 1911 *Phil. Mag.* **21** 669
[2] Egerton R F 1996 *Electron Energy Loss Spectroscopy in the Electron Microscope* (New York: Plenum) and references therein
[3] Spence J C H 2003 *High-Resolution Electron Microscopy* (New York: Oxford University Press)
[4] Mayol R and Salvat F 1997 *At. Data Nucl. Data Tables* **65** 55
[5] Rose H H 2008 *Sci. Technol. Adv. Mater.* **9** 014107
[6] Tanaka N 2008 *Sci. Technol. Adv. Mater.* **9** 014111
[7] Kaiser U, Muller D A, Grazul J L, Chuvilin A and Kawasaki M 2002 *Nat. Mater.* **1** 102
[8] Varela M *et al* 2004 *Phys. Rev. Lett.* **92** 95502
[9] Bals S, Kilaas R and Kisielowski C 2005 *Ultramicroscopy* **104** 281
[10] Wang Z L 1999 *Phil. Mag.* B **79** 37
[11] Hartel P, Rose H and Dinges C 1996 *Ultramicroscopy* **63** 93
[12] Furuya K 2008 *Sci. Technol. Adv. Mater.* **9** 014110
[13] Song M and Furuya K 2008 *Sci. Technol. Adv. Mater.* **9** 023002
[14] Iakoubovskii K, Mitsuishi K and Furuya K 2008 *Nanotechnology* **19** 155705
[15] Iakoubovskii K, Mitsuishi K, Nakayama Y and Furuya K 2008 *Phys. Rev.* B **77** 104102
[16] Iakoubovskii K, Mitsuishi K, Nakayama Y and Furuya K 2008 *Microsc. Res. Tech.* **71** 626
[17] Iakoubovskii K and Mitsuishi K 2008 *Phys. Rev.* B **78** 064105
[18] Mano T and Koguchi N 2005 *J. Cryst. Growth* **278** 108
[19] Larsen F K, Lehmann M S and Merisalo M 1980 *Acta Crystallogr.* A **36** 159
[20] Metzger T H 1986 *J. Appl. Crystallogr.* **19** 200
[21] Sledziewska-Blocka D and Lebech B 1976 *Acta Crystallogr.* A **32** 150
[22] Singh N and Sharma P R 1971 *Phys. Rev.* B **3** 1141
[23] Skelton E F and Katz J L 1968 *Phys. Rev.* **171** 801
[24] Rossmanith E 1978 *Acta Crystallogr.* A **34** 497
[25] Katmal M and Malik S S 1978 *Phys. Rev.* B **18** 1609

[26] Bashir J, Khan Q H and Butt N M 1987 *Acta Crystallogr.* A **43** 795
[27] Fischer P, Sosnowska I and Szymanski M 1978 *J. Phys. C: Solid State Phys.* **11** 1043
[28] Skelton E F 1969 *J. Appl. Crystallogr.* **2** 106
[29] Gopi Krishna N and Sirdeshmukh D B 1983 *Phys. Status Solidi* b **116** k105
[30] Graf M J 2007 *J. Alloys Compounds* **444/445** 268
[31] Higashimine K, Tajima K and Mitani T 2007 *Sci. Technol. Adv. Mater.* **8** 282
[32] Xu S, Shangguan W, Yuan J, Shi J and Chen M 2007 *Sci. Technol. Adv. Mater.* **8** 40
[33] Tian M, Shangguan W, Yuan J, Wang S and Ouyang Z 2007 *Sci. Technol. Adv. Mater.* **8** 82
[34] Lin K-S, Chang N-B and Chuang T-D 2008 *Sci. Technol. Adv. Mater.* **9** 025015